Magnetic levitation for effective loading of cold cesium atoms in a crossed dipole trap

Yuqing Li,[1] Guosheng Feng,[1] Rundong Xu,[1] Xiaofeng Wang,[1] Jizhou Wu,[1] Gang Chen,[1] Xingcan Dai,[2] Jie Ma,[1,*] Liantuan Xiao,[1] and Suotang Jia[1]

[1]*State Key Laboratory of Quantum Optics and Quantum Optics Devices, Institute of Laser Spectroscopy, College of Physics and Electronics Engineering, Shanxi University, Taiyuan 030006, China*

[2]*State Key Laboratory for Low-Dimensional Quantum Physics, Department of Physics, Tsinghua University, Beijing 100084, China*

(Received 28 January 2015; published 6 May 2015)

We report a detailed study of effective magnetically levitated loading of cold atoms in a crossed dipole trap: an appropriate magnetic field gradient precisely compensates for the destructive gravitational force of the atoms and an additional bias field simultaneously eliminates the antitrapping potential induced by the magnetic field gradient. The magnetic levitation is required for a large-volume crossed dipole trap to form a shallow but very effective loading potential, making it a promising method for loading and trapping more cold atoms. For cold cesium atoms in the $F = 3, mF = 3$ state prepared by three-dimensional degenerated Raman sideband cooling, a large number of atoms $\sim 3.2 \times 10^6$ have been loaded into a large-volume crossed dipole trap with the help of the magnetic levitation technique. The dependence of the number of atoms loaded and trapped in the dipole trap on the magnetic field gradient and bias field, respectively, is in good agreement with the theoretical analysis. The optimum magnetic field gradient of 31.13 G/cm matches the theoretical value of 31.3 G/cm well. This method can be used to obtain more cold atoms or a large number of Bose-Einstein condensation atoms for many atomic species in high-field seeking states.

DOI: 10.1103/PhysRevA.91.053604 PACS number(s): 37.10.De, 37.10.Gh, 85.70.Rp

I. INTRODUCTION

Optical dipole traps are used extensively for preparing and trapping cold dense atomic samples [1]. They can create a variety of trapping potentials [2] and therefore offer the possibility to study numerous physical situations such as double-well potentials [3–6], microscopic traps [7–10], and optical lattices [11–14]. Moreover, they have many advantages over magnetic traps since the magnetic field can be used as a degree of freedom [15–19]. As a consequence, they are crucial to the study of Bose-Einstein condensations (BEC) with internal spin degrees of freedom [15,20], magnetically tunable Feshbach resonances [21,22], and formation of cold molecules [23,24]. Last but not least, for some atomic species, condensation in a magnetic trap is not possible and all-optical trapping and cooling is necessary. This is the case for magnetically untrappable atoms such as ytterbium [25] or alkaline-earth atoms [26,27] and also for cesium atoms because of their large inelastic collision rate [28,29].

To prepare a large number of atoms in an optical trap for further exploration, it must be possible to load and trap cold atoms in a large-volume crossed dipole trap [29]. Considering the laser power limitation, large-volume dipole traps formed by laser beams with a large waist are often "shallow." An essential prerequisite for trapping atoms is that the temperature of the atomic sample is sufficiently lower than the trap depth. Many elaborated strategies have been used to obtain an atomic sample at low temperature. Compressed magneto-optical trap (CMOT) and optical molasses have been employed to obtain a cold atomic cloud at a few tens of microkelvins [15–19]. Furthermore, three-dimensional (3D) degenerated Raman sideband cooling (DRSC) has been applied to prepare Cs atoms in the $F = 3, mF = 3$ state at a low temperature of around 1 μK, which also suppresses inelastic endothermic two-body collision loss [28,29]. Although one can obtain an atomic sample with a sufficiently low temperature, it is sometimes difficult to load and trap a large number of atoms in a large-volume dipole trap [30,31] due to the destructive potential created by the gravity of atoms. Especially for Cs atoms, the vertical gravitational potential gradient of 157 μK/mm is usually much stronger than the loading potential gradient of a large-volume dipole trap. A feasible method is to employ the magnetic levitation technique as compensation for the gravitational force, in which a magnetic field gradient is applied to compensate for the gravitational force and an additional uniform bias field is simultaneously needed to eliminate the antitrapping potential induced by the magnetic field gradient.

More recently, magnetic levitation has been employed as one vital and indispensable step in several experiments to load and trap more cold atoms in a large-volume dipole trap. The experiments include a Cs BEC obtained in an optical trap [28,29], an accelerated evaporative cooling for Cs BEC [32], and a measurement of interspecies ^{6}Li - ^{133}Cs Feshbach resonances [33]. In the experiments mentioned above, both a fixed magnetic field gradient of 31.3 G/cm calculated from theory and a bias field of >50 G have been applied. However, the effect of magnetically levitated fields on the number of atoms loaded and trapped in the dipole trap still lacks a detailed experimental investigation. The dynamic evolution and quantitative theoretical analysis have not yet been well understood and studied in detail. Due to advancements in cold atoms and all-optical BEC experiments, it is essential to carry out more accurate studies on the effect of magnetically levitated fields on the number of atoms loaded and trapped in a large-volume dipole trap.

In this paper, we study the magnetically levitated loading of cold atoms in a large-volume crossed dipole trap in detail. Theoretical loading potentials are presented for a variety

*mj@sxu.edu.cn

of magnetic field gradients and bias fields. Then magnetic levitation is applied to load and trap Cs atoms with a relatively low initial temperature obtained by 3D DRSC in a large-volume dipole trap. The dependence of the number of trapped atoms on a variety of magnetic field gradients and bias fields is measured, which is in good agreement with the theory. In addition, a strong three-body recombination loss is observed, which leads to a fast and strong loss for atoms trapped in the magnetically levitated dipole trap. This paper is organized as follows. In Sec. II we present the theoretical analysis and in Sec. III we describe the experimental setup and processes. The experimental results are given in Sec. IV and the conclusion is presented in Sec. V.

II. THEORETICAL ANALYSIS

This section discusses the loading potential of a typical magnetically levitated dipole trap. We derive the expression of the loading potential induced by the combination of an optical field, a magnetic gradient field, and a bias field. Theoretical evolution of the loading potential in the vertical and horizontal directions with different magnetically levitated fields is given. The parameters used in the theoretical analysis will be shown in Sec. III. These theoretical analyses will be used for the fitting of the experimental results in Sec. IV.

A. Crossed dipole traps

The trapping potential induced by a Gaussian laser beam is proportional to the laser intensity [2,34] and can be expressed as

$$U = -\frac{3Pc^2}{\omega_0^3 \mathrm{w}(x)^2}\left(\frac{\Gamma}{\omega_0-\omega}+\frac{\Gamma}{\omega_0+\omega}\right)e^{-2r^2/\mathrm{w}^2(x)}, \qquad (1)$$

where c is the speed of light, Γ is the natural line width, ω is the frequency of the dipole trap laser, ω_0 is an effective transition frequency defined by a weighted average of both D lines for cesium atoms, P is the total laser power, x is the axial coordinate along the beam axis, and r is the radial coordinate. The position-dependent beam waist $\mathrm{w}(x)$ follows the relation

$$\mathrm{w}(x) = \mathrm{w}_0\sqrt{1+\left(\frac{x}{z_\mathrm{R}}\right)^2}. \qquad (2)$$

Here w_0 denotes the minimum beam waist at the focus, and the Rayleigh range $z_\mathrm{R} = \pi \mathrm{w}_0^2/\lambda$ is a measurement of the axial extension of the focal region. As we have taken care to avoid the interference effects between two laser beams by maintaining a large frequency difference, the total optical potential is just the sum of the potentials of the laser beams [2,29]. We define the propagation directions of two beams at an angle of 90° as x and y axes. So the optical potential produced by a crossed dipole trap is governed by

$$U_0(x,y,z) = -\frac{3c^3}{\omega_0^3}\left(\frac{\Gamma}{\omega_0-\omega}+\frac{\Gamma}{\omega_0+\omega}\right) \times\left[\frac{P_1}{\mathrm{w}^2(x)}e^{-2(y^2+z^2)/\mathrm{w}^2(x)} +\frac{P_2}{\mathrm{w}^2(y)}e^{-2(x^2+z^2)/\mathrm{w}^2(y)}\right], \qquad (3)$$

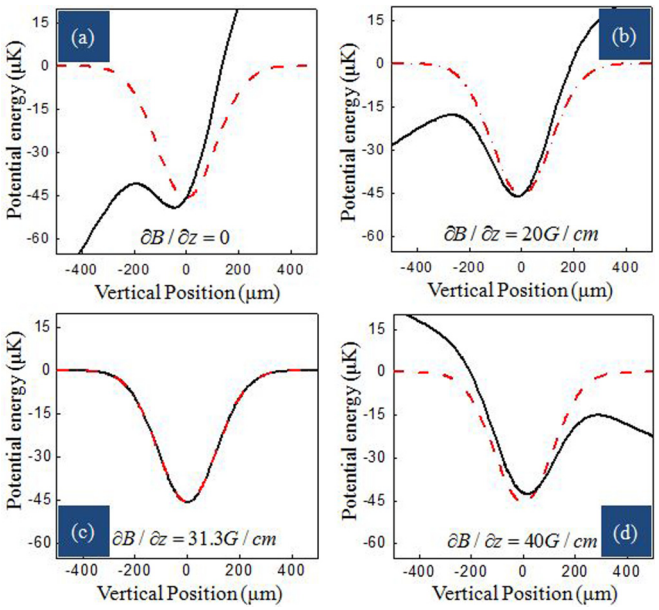

FIG. 1. (Color online) Potentials of a magnetically levitated crossed dipole trap in the vertical direction at the magnetic field gradients of 0 (a), 20 G/cm (b), 31.3 G/cm (c), and 40 G/cm (d). The red dashed line represents the potential of the crossed dipole trap alone, and the black solid line represents the total potential, which includes the destructive potential induced by the gravity of cesium atoms.

where P_1 and P_2 represent the powers of two laser beams of the dipole trap. According to the parameters of our experiment, the numerical results of the optical potential alone are shown in Figs. 1 and 2 along the vertical and horizontal directions, respectively.

B. Magnetic levitation in the vertical direction

Cesium atoms have the largest mass among all nonradioactive alkali metal atoms used to create cold atoms as shown in Table I and are also well suited for cooling and trapping methods. During the process of loading the dipole trap, the gravity of the cesium atoms leads to a potential gradient

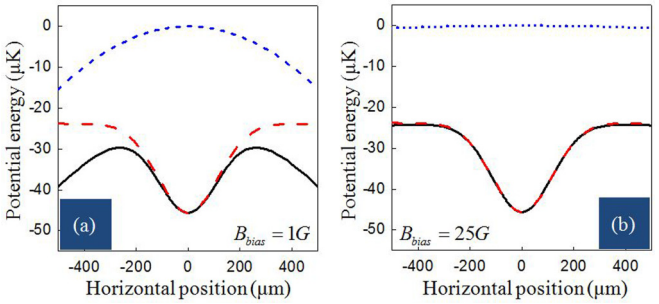

FIG. 2. (Color online) Potentials of a magnetically levitated crossed dipole trap along one of the dipole trap beams at the bias fields of 1 G (a) and 25 G (b). The red dashed line represents the potential of the dipole trap alone, the blue dotted line represents the antitrapping potential produced by the magnetically levitated fields alone, and the black solid line represents the total potential.

TABLE I. The mass and potential gradient induced by the gravity of the nonradioactive alkali metal atoms.

Alkali metal	Mass (10^{-26}kg)	Potential gradient (μK/mm)
^{6}Li	1.00	7.11
^{7}Li	1.17	8.30
^{23}Na	3.84	27.26
^{40}K	6.68	47.42
^{85}Rb	14.20	100.76
^{87}Rb	14.53	103.13
^{133}Cs	22.21	157.66

of 157 μK/mm in the vertical direction, which induces a large destructive potential [29]. The influence of the gravity is very strong and extra care should be taken to compensate for the destructive potential. The magnetic force produced by a magnetic field gradient has been proposed to compensate for the gravity [28,29,32,33,35]. Due to the small efficient space formed by the two crossing focused dipole trap laser beams, the optical potential in the vertical direction could be approximate to $U_0(0,0,z)$. Considering the potential produced by the combination of the gravitational force and the magnetic force, the total potential in the vertical direction is given as

$$U_z = U_0(0,0,z) + mgz + \mu_B m_F g_F \frac{\partial B}{\partial z} z. \tag{4}$$

where g is the gravitational acceleration, μ_B is the Bohr magneton, g_F is the Landé factor, and $\frac{\partial B}{\partial z}$ denotes the magnetic field gradient.

According to Eq. (4), the influence of the magnetic field gradient on the total potential in the vertical direction for cesium atoms in the $F = 3, mF = 3$ state is shown in Fig. 1. It is clear that the destructive potential is so large that there is not an effective potential for trapping atoms when the magnetic field gradient is equal to zero, as shown in Fig. 1(a).

Figure 1(b) gives the potential curve at the magnetic field gradient of 20 G/cm, which indicates that the total potential increases with the magnetic field gradient. In order to completely cancel out the destructive potential induced by the gravity, a magnetic field gradient of 31.3 G/cm is theoretically obtained by considering the relation of $mg + \mu_B m_F g_F \frac{\partial B}{\partial z} = 0$, as shown in Fig. 1(c). With further increases in the magnetic field gradient, the destructive potential will be formed again, as shown in Fig. 1(d). This can be used to reduce the effective potential in an accelerating evaporative cooling process [32].

C. Antitrapping potential along the horizontal direction

According to Maxwell's equation $\nabla \cdot \mathbf{B} = 0$, the application of the vertical magnetic field gradient used to compensate for the gravity inevitably leads to a horizontal magnetic field gradient $\partial B_x/\partial x = \partial B_y/\partial y = (2/3)mg/\mu_B$ in the case of cylindrical symmetry. Unfortunately, this horizontal magnetic field gradient causes an outward pointing force acting on the atoms trapped in the dipole trap and this force leads to an antitrapping potential along the horizontal direction. In order to eliminate the influence of the antitrapping potential along the horizontal direction induced by the magnetic field gradient, a bias field $\mathbf{B}_{\text{bias}}$ must be applied in the vertical direction [29]. Due to the symmetry of anti-Helmholtz coils used to produce the magnetic gradient field, the quadrupole field vector lies in the x-y plane at $z = 0$ and points radially outward from the trap center. The corresponding field strength can be expressed as $B_{\text{grad}}(r) = (2/3)mgr/\mu_B$, and $r = \sqrt{x^2 + y^2}$ is the radial coordinate. Because $\mathbf{B}_{\text{grad}}$ is perpendicular to the vertical bias field $\mathbf{B}_{\text{bias}}$, the strength of the combined magnetic field can be written as

$$B(r) = \sqrt{B_{\text{bias}}^2 + \left(\frac{2mgr}{3\mu_B}\right)^2} \approx B_{\text{bias}}\left[1 + \frac{1}{2}\left(\frac{2mgr}{3\mu_B B_{\text{bias}}}\right)^2\right] = B_{\text{bias}} + \frac{2}{9}\frac{m^2 g^2 r^2}{\mu_B^2 B_{\text{bias}}}. \tag{5}$$

The magnetic potential along the horizontal direction is calculated as

$$U_B(r) = -\frac{3}{4}\mu_B B(r) = -\frac{3}{4}\mu_B B_{\text{bias}} - \frac{1}{6}\frac{m^2 g^2}{\mu_B B_{\text{bias}}} r^2. \tag{6}$$

The shallow potential of a large-volume dipole trap allows the optical potential along the horizontal direction to approximate to $U_0(x,y,0)$ in a small efficient space.

By combining the optical potential and the antitrapping magnetic potential, the total potential along the horizontal direction can be given as

$$U_r = U_0(x,y,0) - \frac{3}{4}\mu_B B(r) = U_0(x,y,0) - \frac{3}{4}\mu_B B_{\text{bias}} - \frac{1}{6}\frac{m^2 g^2}{\mu_B B_{\text{bias}}}(x^2 + y^2). \tag{7}$$

According to Eq. (7), the antitrapping potential in the horizontal direction can be reduced by adding a bias field in the vertical direction. Figure 2 gives the potential of the magnetically levitated dipole trap along one of the dipole trap beams at different bias fields. When a small bias field of ~1 G is applied, the antitrapping potential is still very large, as shown in Fig. 2(a). When the bias field reaches the value of ~25 G, the antitrapping potential has decreased to nearly zero and therefore the total potential along the horizontal direction is almost equal to the optical potential induced by the dipole trap alone in Fig. 2(b). If we continue to increase the bias field, the antitrapping potential becomes closer and closer to the infinitesimal but not zero according to Eq. (7).

III. EXPERIMENTAL SETUP

A. MOT and 3D DRSC

The experimental setup is shown schematically in Fig. 3. The cold Cs atoms are produced in a single cell with a high vacuum of ~2.5×10^{-8} Pa by a standard vapor-loaded MOT. The temperature of the atomic sample is measured as about 200 μK by the time-of-flight (TOF) method [36]. The number of trapped atoms is about 9×10^7.

After the loading of the MOT, the CMOT and optical molasses are performed by increasing the magnetic field gradient, reducing the repumping laser power, and increasing the trapping laser frequency detuning. A further added laser cooling step, namely 3D DRSC [37,38], is very efficient for trapped atoms in our experiment. As shown in Fig. 3, the atoms

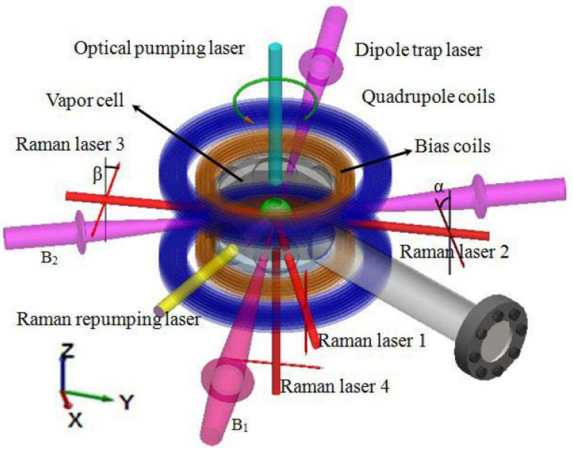

FIG. 3. (Color online) Experimental setup for the magnetically levitated crossed dipole trap. The positions of vacuum cell, laser beams for 3D DRSC (Raman lasers 1–4, Raman repumping laser, and optical pumping laser) and crossed dipole trap lasers (B1 and B2), and two pairs of magnetic field coils are presented.

are transferred and captured in a 3D optical lattice that consists of four linearly polarized laser beams, which guarantees the stabilization of the optical lattice [39]. The detailed description of the 3D DRSC can be found in Ref. [38]. The optical lattice lights are switched on at 0.5 ms before the end of the optical molasses process to load and trap cold atoms [40]. The DRSC is subsequently implemented on the atoms in the stationary 3D optical lattice for 10 ms. At the end of the 3D DRSC, for the adiabatic release of the optical lattice, the lattice power P is decreased according to $P(t) = P(0)[1 + t/t_0]^{-2}$, where the typical value of t_0 is 100 μs [37,38,41].

B. Crossed dipole traps

To transfer more cold Cs atoms into a dipole trap, we superimpose a large-volume crossed dipole trap on the atomic sample released from the optical lattice in the 3D DRSC. The dipole trap is produced by a 1070-nm, multifrequency, linearly polarized fiber laser (IPG Photonics). This dipole trap consists of two horizontally crossing beams, B_1 and B_2, at an angle of 90°, as shown in Fig. 3. The delivered powers of laser beams B_1 and B_2 are 7 and 7.2 W, respectively. The two laser beams B_1 and B_2 are weakly focused on the trap center with beam waists of $w_x = 230\,\mu$m and $w_y = 240\,\mu$m. There are two acousto-optical modulators (Crystal Technology) with 110 MHz frequency shifts used in intensity stabilization and rapid switching off in less than 1 μs for two dipole trap laser beams. B_1 is downshifted in frequency by 110 MHz, whereas B_2 is upshifted by 110 MHz to prevent any interference between the two dipole trap laser beams. At the same time we apply a magnetic gradient field and a bias field to compensate for the antitrapping potentials in the vertical and horizontal directions during the loading of the dipole trap.

C. Magnetic levitation

The magnetically levitated loading of a large-volume dipole trap is implemented by employing a magnetic field gradient to compensate for the gravitational force and an additional bias field to eliminate the antitrapping potential induced by the magnetic field gradient. The magnetic field gradient is produced by a pair of anti-Helmholtz coils used for the MOT. In Fig. 3 the outer pair of coils is the anti-Helmholtz coils, which consist of many copper tube windings with an outside diameter of 4 mm, and each of the coils has a total of 35 turns. Their radius and distance are chosen as $R = 1.2$ cm and $D = 90$ cm, which is a result of a compromise between a homogenous gradient and a large gradient strength. We can obtain a maximum gradient of 61 G/cm at a current of 60 A. Due to a large ramping time of 7.5 ms for the loading of the current in anti-Helmholtz coils, we add a resistance of 0.5 Ω in series in the coils whose resistance is 0.1 Ω, and the ramping time then decreases to 1.2 ms. The bias field is provided by a pair of Helmholtz coils. The inner pair of coils is the Helmholtz coils, which consist of many copper tube windings with the same outside diameter of 4 mm, as shown in Fig. 3. Each of the two Helmholtz coils has 20 turns. We choose the radius R and the distance D as $R = 0.93$ cm and $D = 65$ cm so that they can produce a uniform magnetic field in a relatively wide range near the center of this pair of coils. The Helmholtz coils are designed to provide a magnetic field of up to 175 G at a current of 40 A. These two pairs of coils are mounted around the high-vacuum cell and assembled along the vertical direction. It is also necessary to superimpose the center of the coils on the trapped atomic sample. The water cooling, which allows a high current to flow in the coils for a long time, is applied to the two pairs of coils by the water flowing in the copper tubes.

IV. EXPERIMENTAL RESULTS

A. Preparation of cold Cs atoms

We have obtained 3×10^7 atoms with a peak density of around 10^{11} cm^{-3} using the CMOT and optical molasses. The temperature of atoms obtained in our experiment is $T = 60\,\mu$K by conventional optical molasses in the $F = 4$ state. This temperature is relatively high compared with that obtained from the optical molasses cooling following the MOT loaded by a Zeeman slower or blue detuned Sisyphus cooling in the $F = 3$ state [28,29,32,33,41]. After the 3D DRSC we obtain the cold atoms with a low temperature of $T = 1.7\,\mu$K. The absorption image is taken in the horizontal direction after 12 ms of expansion following the release of the 3D optical lattice as shown in Fig. 4. Here the measured atomic number is about 1.7×10^7, the proportion of the atoms in the $F = 3, mF = 3$ state is about 75%, and the other atoms are mainly in the $F = 3, mF = 2$ state, which can be distinguished by applying a Stern-Gerlach magnetic field.

B. Detection for loading of crossed dipole trap

The atoms, prepared by 3D DRSC, can be loaded into the crossed dipole trap as much as possible with the help of magnetic levitation. The detection for the loading of the magnetically levitated crossed dipole trap is achieved by monitoring the number of atoms loaded and held in the dipole trap, as shown in Fig. 5. We use absorption imaging to measure the remaining atoms in the dipole trap after 30 ms of

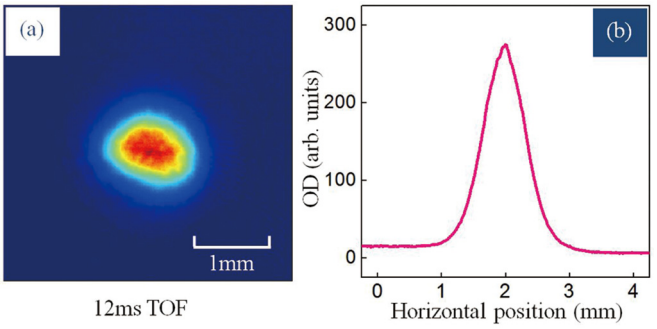

FIG. 4. (Color online) (a) Absorption image taken along the horizontal direction after 12 ms of TOF following the release of the 3D DRSC. (b) The corresponding distribution of optical density (OD) along the horizontal direction.

evaporation with a large scattering length $a = 1230a_0$, where a_0 is the Bohr radius.

The corresponding absorption images are taken in the horizontal and vertical directions after 3 ms of expansion following the release of the dipole trap. The maximum atomic number held in the dipole trap is measured to be 3.2×10^6. The loading procedure is optimized by geometrically overlapping the positions of two dipole laser beams with the atomic cloud released from the 3D optical lattice. This is done by imaging the positions on CCD cameras with a resolution of 9 μm; if the two dipole laser beams are close to the atomic cloud, they lead to a local increase in density. With one camera looking in the horizontal direction and the other looking in the vertical direction, we have full spatial information and can slightly adjust the positions of two dipole laser beams using high precision mirrors. The spatial distribution of the atoms trapped in the dipole trap is dominated by a Gaussian function, and the corresponding $1/e$ radii are 136 μm and 139 μm in Figs. 5(a) and 5(b), respectively.

C. Magnetic field gradient dependence

We have studied the dependence of the number of atoms trapped in the dipole trap on the magnetic field gradient with a bias field of $B_{\text{bias}} = 75$ G. The number of the atoms is measured after 30 ms of evaporation following the loading

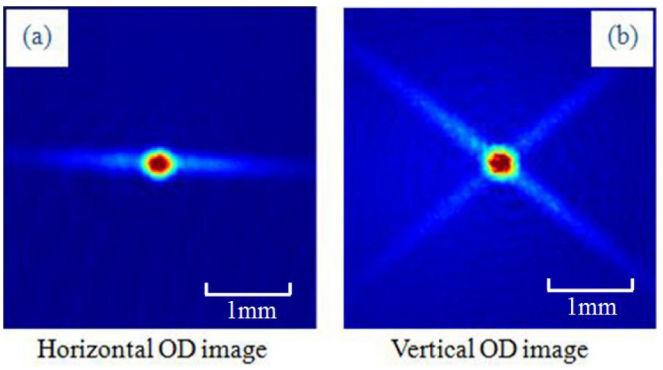

FIG. 5. (Color online) Absorption images (a) and (b) taken along the horizontal and vertical directions, respectively, after 3 ms of TOF following the release of the magnetically levitated crossed dipole trap.

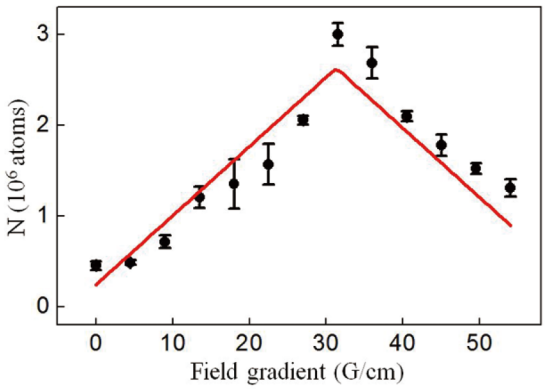

FIG. 6. (Color online) Number of atoms in the magnetically levitated dipole trap as a function of magnetic field gradient. The red line is a fitting curve according to Eq. (4).

of the dipole trap. The magnetic field gradient $\frac{\partial B}{\partial z}$ is firstly ramped up to a value of 45 G/cm in 1.5 ms, which is more than that is needed to counteract the gravity. The magnetic field gradient is then relaxed to a final value within 2 ms. This deliberate levitation overshoot compensates for the finite ramping speed of the magnetic field gradient and cancels the atomic downward velocity induced by the gravity while the magnetic field gradient is ramped up. At the beginning, with increases in the magnetic field gradient $\frac{\partial B}{\partial z}$ after the overshoot, the number of atoms trapped in the dipole trap presents a linear growth, as shown in Fig. 6. For each data point, all initial parameters of both atomic samples prepared by the 3D DRSC and magnetically levitated dipole trap are kept unchanged in each experimental cycle except for the magnetic field gradient and bias field in Figs. 6 and 7, respectively.

According to the dependence of the number of trapped atoms on the trap depth as shown in Ref. [34], the number of trapped atoms is proportional to the trap depth of a shallow dipole trap under our experimental conditions. Here we use Eq. (4) to fit the experimental data by introducing a ratio constant, which describes the relation between the depth of the magnetically levitated dipole trap and the number of trapped atoms. The difference between the measured data and the fitting line is mainly attributed to the fact that all

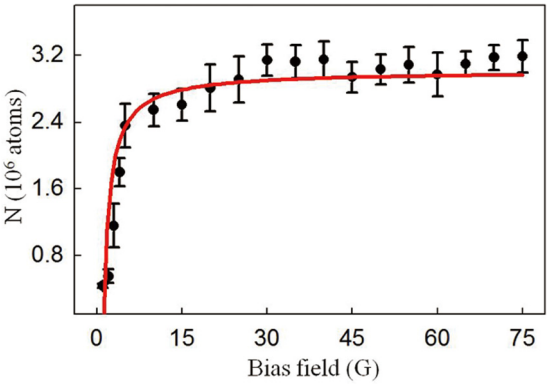

FIG. 7. (Color online) Number of atoms in the magnetically levitated dipole trap as a function of bias field. The red line is a fitting curve according to Eq. (7).

of the atoms cannot be trapped uniformly in the magnetically levitated dipole trap. When the magnetic field gradient reaches the value of 31.13 G/cm, the number of trapped atoms will decrease with further increase of the magnetic field gradient. Thus, it can be easily understood that the further increase of magnetic field gradient leads to the result that the destructive potential appears again and increases since the magnetic field gradient exceeds the value of 31.13 G/cm. It is worth noting that the value of 31.13 G/cm is in good agreement with the theoretical value of 31.3 G/cm, in which the magnetic force can precisely compensate for the gravitational force.

D. Bias field dependence

In order to study the influence of the antitrapping potential along the horizontal direction induced by the magnetic field gradient on the number of atoms loaded and trapped in the magnetically levitated dipole trap, the magnetic field gradient is fixed at $\frac{\partial B}{\partial z} = 31.13$ G/cm to completely compensate for the gravity. The variation of atomic number in the dipole trap with an increasing bias field is shown in Fig. 7. The atomic number is measured after 30 ms of evaporation following the loading of the dipole trap.

Equation (7) is used to fit the experimental data by introducing a proportional constant that makes a good connection between the number of trapped atoms and the total potential depth. At the beginning, with the increase of the bias field B_{bias}, the atomic number in the dipole trap has a large growth rate. However, the growth rate becomes very low after the bias field reaches 10 G. When the bias field approaches 30 G, the atomic number stops increasing. Normally the bias field used in the loading process of the dipole trap should be greater than $B_{\text{bias}} = 30$ G.

E. Magnetically levitated crossed dipole trap and large three-body loss

We find that the atoms are heated to $T = 8.9$ μK in the process of transforming into the magnetically levitated dipole trap. The heating is mainly attributed to the imperfect space matching in the loading process. The optical lattice beams in the 3D DRSC have a $1/e$ radius of ~1.15 mm. In comparison, the dipole trap beams have a $1/e$ radius of ~240 μm. The potential energy is thus gained and then turned into kinetic energy, which heats the atomic sample. Subsequently, the hot atoms escape out of the dipole trap in plain evaporation. For this phase of plain evaporation the bias field is tuned to $B_{\text{bias}} =$ 75 G and the corresponding scattering length is $a = 1230a_0$. The temperature is reduced to less than $T = 3.8$ μK within 600 ms. The measured atomic number is 2.5×10^5 and the density is a few 10^{11} cm^{-3}. In Fig. 8(a) the absorption image is taken in the horizontal direction after 3 ms of TOF following the release of the dipole trap and the corresponding distribution of optical density is shown in Fig. 8(b).

For cesium atoms in the magnetically levitated dipole trap, the atomic number is measured as a function of storage time as shown in Fig. 9. A strong loss has been observed in the initial 300 ms of evaporation. This is mainly attributed to a very strong three-body recombination loss at the bias field of $B_{\text{bias}} = 75$ G [29,30]. Three atoms collide and two of them

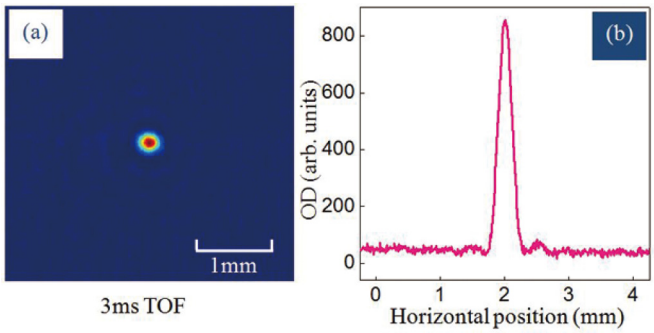

FIG. 8. (Color online) (a) The absorption image taken along the horizontal direction after 3 ms of TOF following the release of the magnetically levitated crossed dipole trap. (b) The corresponding distribution of optical density (OD) along the horizontal direction.

form a molecule. The third atom will take away two thirds of the binding energy and deposits its share of the binding energy in the atomic sample [31].

The atomic number in the dipole trap is measured as about 3.2×10^6 after 30 ms of evaporation, but the number is reduced by an order of magnitude after 300 ms of plain evaporation. The change of the number of trapped atoms is relatively small after 300 ms of plain evaporation. This is mainly attributed to a sharp decrease of the atomic number density in the initial 300 ms of plain evaporation dominated by a strong three-body loss and the local three-body loss rate is proportional to the third power of the atomic number density.

V. CONCLUSION

We have investigated the magnetically levitated loading of cold atoms in a large-volume crossed optical dipole trap in detail. Unlike previous works, we do not use a very deep loading potential with a small laser beam waist of several tens of micrometers to load and trap atoms with a few tens of microkelvins. A large-volume crossed dipole trap is employed to load and trap more atoms at a low temperature obtained by the 3D DRSC with the help of magnetic levitation. After 30 ms of plain evaporation following the magnetically levitated

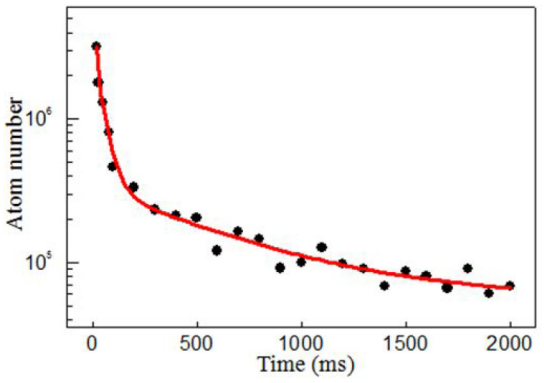

FIG. 9. (Color online) Number of atoms remaining in the magnetically levitated crossed dipole trap as a function of time. The strong three-body loss is observed in 300 ms after the loading of the magnetically levitated crossed dipole trap.

loading, we obtain 3.2×10^6 atoms in the levitated dipole trap. The obtained dependence of the number of trapped atoms on the magnetic field gradient and bias field is in good agreement with our theoretical analysis. Consequently, the magnetic field gradient of 31.13 G/cm obtained from the fitting of experimental data agrees well with the theoretical value of 31.3 G/cm, where the number of atoms trapped in the magnetically levitated dipole trap reaches its maximum. Besides, a strong three-body loss has been observed at a large scattering length of $\sim 1230 a_0$ [30]. The temperature is reduced to 3.8 μK after 600 ms of plain evaporation. The magnetic levitation is expected to load and trap more cold atoms and even BEC atoms for other atomic species in high-field seeking states in large-volume dipole traps. It also allows ones to carry out further researches and applications. For example, we have experimentally observed the controllable photoassociation via a changing bias field and the enhanced photoassociation near a d-wave Feshbach resonance in the magnetically levitated dipole trap.

ACKNOWLEDGMENTS

This work was supported by 973 Program (Grants No. 2012CB921603 and No. 2013CB922003), PCSIRT (Grant No. IRT13076), NSF of China (Grants No. 91436108, No. 61378014, No. 61308023, No. 61121064, No. 61275211, No. 61378015, and No. 11434007).

[1] J. D. Miller, R. A. Cline, and D. J. Heinzen, Phys. Rev. A **47**, R4567(R) (1993).
[2] R. Grimm, M. Weidemüller, and Y. B. Ovchinnikov, Adv. At. Mol. Opt. Phys. **42**, 95 (2000).
[3] M. Saba, T. A. Pasquini, C. Sanner, Y. Shin, W. Ketterle, and D. E. Pritchard, Science **307**, 1945 (2005).
[4] J. Estève, C. Gross, A. Weller, S. Giovanazzi, and M. K. Oberthaler, Nature (London) **455**, 1216 (2008).
[5] A. Gaëtan, Y. Miroshnychenko, T. Wilk, A. Chotia, M. Viteau, D. Comparat, P. Pillet, A. Browaeys, and P. Grangier, Nature Phys. **5**, 115 (2009).
[6] E. Urban, T. A. Johnson, T. Henage, L. Isenhower, D. D. Yavuz, T. G. Walker, and M. Saffman, Nature Phys. **5**, 110 (2009).
[7] R. Bourgain, J. Pellegrino, A. Fuhrmanek, Y. R. P. Sortais, and A. Browaeys, Phys. Rev. A **88**, 023428 (2013).
[8] N. Schlosser, G. Reymond, and P. Grangier, Phys. Rev. Lett. **89**, 023005 (2002).
[9] J. Sebby-Strabley, R. T. R. Newell, J. O. Day, E. Brekke, and T. G. Walker, Phys. Rev. A **71**, 021401(R) (2005).
[10] A. Goban, K. S. Choi, D. J. Alton, D. Ding, C. Lacroûte, M. Pototschnig, T. Thiele, N. P. Stern, and H. J. Kimble, Phys. Rev. Lett. **109**, 033603 (2012).
[11] Th. Best, S. Will, U. Schneider, L. Hackermüller, D. van Oosten, I. Bloch, and D.-S. Lühmann, Phys. Rev. Lett. **102**, 030408 (2009).
[12] L. Hackermüller, U. Schneider, M. Moreno-Cardoner, T. Kitagawa, Th. Best, S. Will, E. Demler, E. Altman, I. Bloch, and B. Paredes, Science **327**, 1621 (2010).
[13] K. C. Younge, B. Knuffman, S. E. Anderson, and G. Raithel, Phys. Rev. Lett. **104**, 173001 (2010).
[14] S. E. Anderson and G. Raithel, Phys. Rev. Lett. **109**, 023001 (2012).
[15] M. D. Barrett, J. A. Sauer, and M. S. Chapman, Phys. Rev. Lett. **87**, 010404 (2001).
[16] A. G. Truscott, K. E. Strecker, W. I. McAlexander, G. B. Partridge, and R. G. Hulet, Science **291**, 2570 (2001).
[17] F. Schreck, L. Khaykovich, K. L. Corwin, G. Ferrari, T. Bourdel, J. Cubizolles, and C. Salomon, Phys. Rev. Lett. **87**, 080403 (2001).
[18] S. R. Granade, M. E. Gehm, K. M. O'Hara, and J. E. Thomas, Phys. Rev. Lett. **88**, 120405 (2002).
[19] A. L. Marchant, S. Händel, S. A. Hopkins, T. P. Wiles, and S. L. Cornish, Phys. Rev. A **85**, 053647 (2012).
[20] J. Stenger, S. Inouye, D. M. Stamper-Kurn, H.-J. Miesner, A. P. Chikkatur, and W. Ketterle, Nature (London) **396**, 345 (1998).
[21] T. Köhler, K. Góral, and P. S. Julienne, Rev. Mod. Phys. **78**, 1311 (2006).
[22] C. Chin, R. Grimm, P. Julienne, and E. Tiesinga, Rev. Mod. Phys. **82**, 1225 (2010).
[23] K.-K. Ni, S. Ospelkaus, M. H. G. de Miranda, A. Pe'er, B. Neyenhuis, J. J. Zirbel, S. Kotochigova, P. S. Julienne, D. S. Jin, and J. Ye, Science **322**, 231 (2008).
[24] S. Ospelkaus, A. Pe'er, K.-K. Ni, J. J. Zirbel, B. Neyenhuis, S. Kotochigova, P. S. Julienne, J. Ye, and D. S. Jin, Nature Phys. **4**, 622 (2008).
[25] Y. Takasu, K. Maki, K. Komori, T. Takano, K. Honda, M. Kumakura, T. Yabuzaki, and Y. Takahashi, Phys. Rev. Lett. **91**, 040404 (2003).
[26] S. Kraft, F. Vogt, O. Appel, F. Riehle, and U. Sterr, Phys. Rev. Lett. **103**, 130401 (2009).
[27] S. Stellmer, M. K. Tey, B. Huang, R. Grimm, and F. Schreck, Phys. Rev. Lett. **103**, 200401 (2009).
[28] T. Weber, J. Herbig, M. Mark, H.-C. Nägerl, and R. Grimm, Science **299**, 232 (2003).
[29] T. Kraemer, J. Herbig, M. Mark, T. Weber, C. Chin, H.-C. Nägerl, and R. Grimm, Appl. Phys. B **79**, 1013 (2004).
[30] T. Weber, J. Herbig, M. Mark, H.-C. Nägerl, and R. Grimm, Phys. Rev. Lett. **91**, 123201 (2003).
[31] R. Pires, J. Ulmanis, S. Häfner, M. Repp, A. Arias, E. D. Kuhnle, and M. Weidemüller, Phys. Rev. Lett. **112**, 250404 (2014).
[32] C. L. Hung, X. B. Zhang, N. Gemelke, and C. Chin, Phys. Rev. A **78**, 011604 (2008).
[33] M. Repp, *Interspecies Feshbach Resonances in an Ultracold, Optically Trapped Bose-Fermi Mixture of Cesium and Lithium* (University of Heidelberg, Germany, 2013).
[34] S. J. M. Kuppens, K. L. Corwin, K. W. Miller, T. E. Chupp, and C. E. Wieman, Phys. Rev. A **62**, 013406 (2000).

[35] D. L. Jenkina, D. J. McCarron, M. P. Köppinger, H. W. Cho, S. A. Hopkins, and S. L. Cornish, Eur. Phys. J. D **65**, 11 (2011).

[36] W. Ketterle, D. S. Durfee, and D. M. Stamper-Kurn, in *Bose-Einstein Condensation in Atomic Gases, Proceedings of the International School of Physics "Enrico Fermi," Course CXL*, edited by M. Inguscio, S. Stringari, and C. E. Wieman (IOS Press, Amsterdam, 1999), pp. 67–176.

[37] A. J. Kerman, V. Vuletić, C. Chin, and S. Chu, Phys. Rev. Lett. **84**, 439 (2000).

[38] P. Treutlein, K. Y. Chung, and S. Chu, Phys. Rev. A **63**, 051401 (2001).

[39] G. Grynberg, B. Lounis, P. Verkerk, J.-Y. Courtois, and C. Salomon, Phys. Rev. Lett. **70**, 2249 (1993).

[40] M. T. DePue, S. L. Winoto, D. J. Han, and D. S. Weiss, Opt. Comm. **180**, 73 (2000).

[41] V. Vuletić, C. Chin, A. J. Kerman, and S. Chu, Phys. Rev. Lett. **81**, 5768 (1998).